Chiral Spin Spirals at the Surface of the van der Waals Ferromagnet Fe_3GeTe_2

Mariëlle J. Meijer,[1,*] Juriaan Lucassen,[1] Rembert A. Duine,[1,2] Henk J.M. Swagten,[1] Bert Koopmans,[1] Reinoud Lavrijsen,[1] and Marcos H. D. Guimarães[1,3,†]

[1] *Department of Applied Physics, Eindhoven University of Technology, P.O. Box 513, 5600 MB Eindhoven, the Netherlands*

[2] *Institute for Theoretical Physics, Utrecht University, Leuvenlaan 4, 3584 CE Utrecht, the Netherlands*

[3] *Zernike Institute for Advanced Materials, University of Groningen, Nijenborgh 4, 9747 AG Groningen, the Netherlands*

(Dated: November 10, 2020)

SI. SEMPA SETUP AND SEM AND AFM MEASUREMENTS ON FGT

In this section we show a schematic representation of the SEMPA setup as well as additional SEM and AFM images of flake A. A schematic representation of the SEMPA setup is shown in Fig. S1. On the left the scanning electron beam focuses electrons on the sample surface where secondary electrons are emitted. The secondary electrons are accelerated towards a tungsten single-crystal (with crystallographic direction (001)) and scattered into different diffraction spots, depending on their in-plane spin information [S1]. Electron counters are placed at these diffraction spots and images are obtained for the four individual spin directions (m_{x}, $-m_{\mathrm{x}}$, m_{y}, $-m_{\mathrm{y}}$). The contrast images along the two directions (shown in Fig. 1 of the main text) are constructed by the difference in counts of the positive and negative direction detections: $C_{m_{\mathrm{i}}} - C_{-m_{\mathrm{i}}}$ $(i = \mathrm{x}, \mathrm{y})$.

In the SEMPA setup we are able to additionally gain information on the out-of-plane magnetization by tilting the sample. This results in the projection of the magnetization on the in-plane measurement axis, which is adjustable and well-defined for the m_{y} image as depicted schematically in Fig. 1c and d of the main text. In the m_{x} image the out-of-plane projection depends strongly on the sample mounting and flake attachment to the substrate.

To conduct temperature dependent measurements we can cool down the SEMPA stage with liquid nitrogen or helium, resulting in a lowest reachable temperature of 140 K and 60 K, respectively. The FGT flakes are always zero-field cooled, since we are not able to apply any magnetic fields in our SEMPA setup. A heater close to the sample stage allows us to measure at intermediate temperatures.

A SEM image as shown in Fig. S2a is obtained by adding up the counts of all four electron counters and thereby disregarding the spin information. The resolution obtained in this SEM image is identical to the one of the SEMPA images in the main paper (Fig. 1) and features of 30 nm can easily be distinguished. The area studied in the main paper (Fig. 1) is outlined in black and the SEMPA images corresponding to the full area are discussed in Fig. S8.

In Fig. S2b an AFM scan of a large area of the flake is shown. The area measured with SEMPA is outlined in black and the inset shows a detailed scan. The black, green and blue line indicate at which positions the height profiles in Fig. S2c are measured. The green and

* m.j.meijer@tue.nl

† m.h.guimaraes@rug.nl

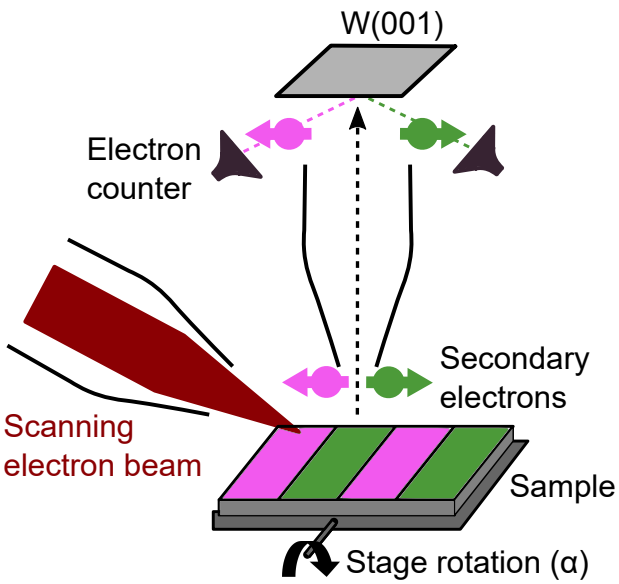

FIG. S1. Schematic of the SEMPA setup. The scanning electron beam hits the sample on a rotatable stage. The secondary electrons are emitted and scatter from the tungsten single-crystal to different diffraction spots according to their spin direction, where electron counters are placed. The figure is adapted from [S2].

black height profile use the y-axis on the left hand side and measure a flake thickness of 185 ± 7 nm. The blue height profile is taken across the area measured with the SEMPA and the y-axis on the right hand side is used. Here, the scale of 0.8 nm corresponds to the thickness of a single FGT layer. Within this height profile and specifically across the narrow crack visible in Fig. S2a and b, we find no height step in the flake.

SII. MAGNETIC CONTRAST IN SEMPA IMAGES

In this section we discuss the differences in magnetic contrast that can be found in the SEMPA images. First, we depict in Fig. S3 that the magnetic contrast in the SEMPA images is greatly enhanced by depositing a thin layer of 0.3 nm of Co on FGT. The SEMPA images of pure FGT are depicted in Fig. S3a and only a very faint contrast in the right SEMPA image, containing the m_{y}-contrast, is visible. In Fig. S3b the same area is imaged after 0.3 nm of Co is deposited on FGT (see main paper for details). Here, the defect in the lower left corner of Fig. S3a corresponds to the defect in the middle of the image of Fig. S3b. The magnetic contrast in Fig. S3b is greatly enhanced and a clear magnetic signal is found

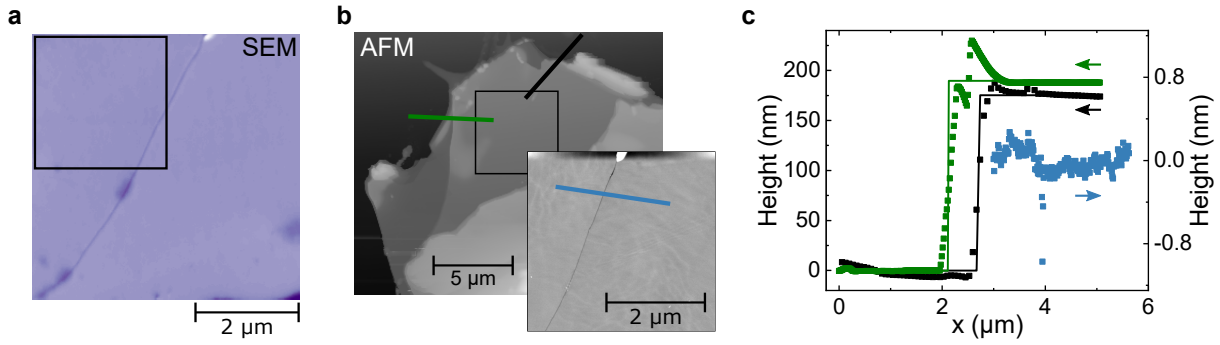

FIG. S2. **a** SEM image measured with SEMPA. The area indicated by the black outline was discussed in the main paper in Fig. 1 and the magnetic contrast in the full area is shown in Fig. S8. **b** AFM images of the sample discussed in the main paper (Fig. 1). An overview scan is depicted as well as a detailed scan (inset) of the area measured with SEMPA. **c** Height profiles of the flake with the location of the line traces indicated in **b**.

showing horizontal lines. In the right SEMPA images of Fig. S3a and b the magnetic contrast is further analyzed in Fig. S3c and d, where the data in the red highlighted area is averaged along the vertical direction. In both graphs a periodic behavior is found, but the amplitude of the oscillations is much stronger in Fig. S3d due to the added Co. We fit both data sets with a sinusoidal function (black lines) and find a similar periodicity of the magnetic signal, which indicates that the thin layer of Co does not induce a magnetic pattern on its own but rather follows the magnetic texture of FGT. This statement is confirmed by the fact that as soon as the Curie-temperature of FGT is reached, the magnetic contrast vanishes entirely (see Fig. 3a of the main paper).

In the second part we discuss the differences in magnetic contrast within SEMPA images. A clear example is depicted in Fig. S4, where a pristine area of an FGT flake is depicted. The left SEMPA image (m_x contrast) shows a very strong magnetic contrast in the upper right hand corner of the image and almost no magnetic contrast in the bottom left hand corner. In the right SEMPA image (m_y contrast) the opposite is observed. From this figure we find that in FGT a strong in-plane magnetization contrast in m_x or m_y corresponds to a magnetic pattern aligned either vertically or horizontally.

The m_z component, which might be present in both SEMPA images, can only be adjusted in the m_y SEMPA image when rotating the sample stage. In order to obtain as much information of the SEMPA images as possible we study in particular the vertically aligned

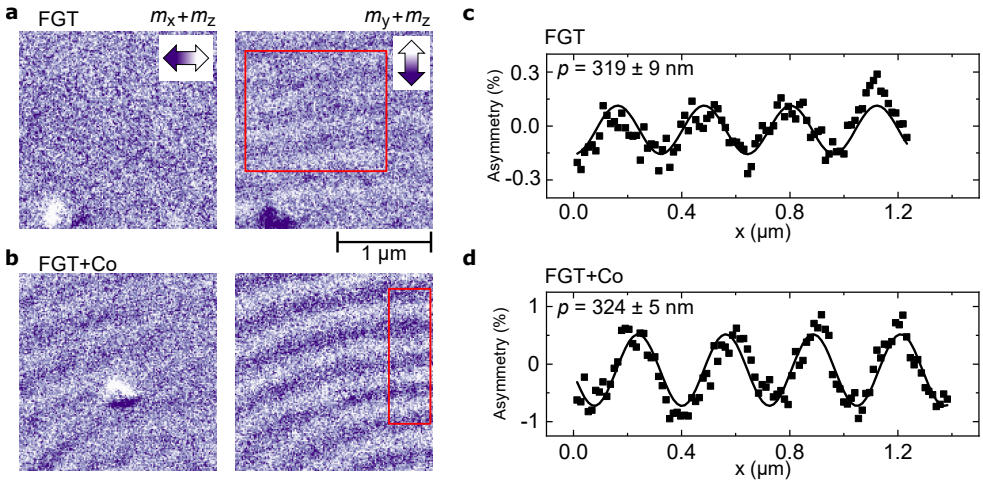

FIG. S3. **a** SEMPA images of FGT with the horizontal and vertical in-plane magnetization depicted in the left and right image, respectively. **b** SEMPA images of the same area after 0.3 nm of Co is deposited on FGT. **c,d** Average magnetic contrast data along the vertical direction of the red rectangle indicated in the SEMPA images. The data are fitted with a sinusoidal function (black line) and a similar periodicity p is extracted. The defects in panel a and b are the same.

magnetic patterns. Here, the main component of the in-plane magnetization will be present in the m_x SEMPA image. A small m_z component in this image can not be differentiated due to the higher sensitivity of the SEMPA for in-plane components. The other SEMPA image then consists of a (small) m_y and m_z magnetization contribution, which can be separated by rotating the sample (see main paper for details).

SIII. ADDITIONAL α DEPENDENT MEASUREMENTS

Fig. S5 shows the dependence of the m_x and m_y contrast on the sample tilt angle α, as shown in Fig. 1 of the main text. Here, we also include the data for $\alpha = +6°$ and $\alpha = -2°$. Note that the uncertainty with which we can determine α is $\pm 2°$. For $\alpha = -2°$ only the in-plane component should be present. Here we observe that while the m_x image and line trace remain relatively unchanged, the contrast for the m_y image vanishes. As explained in the main text, the vanishing of the m_y signal at $\alpha = -2°$ combined with the sign change in the phase shift between the m_x and my channels obtained at $\alpha = +6°$ and $\alpha = -4°$ indicate that the signal in m_y arises from an out-of-plane (m_z) magnetic signal projected on

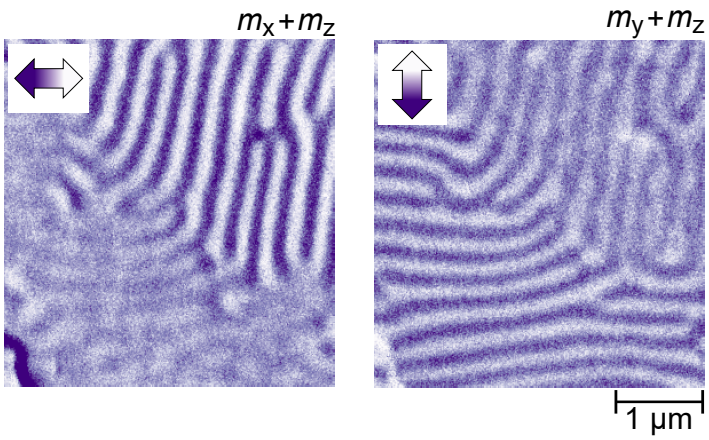

FIG. S4. SEMPA images of FGT with the horizontal and vertical in-plane magnetization depicted in the left and right image, respectively. The area in the upper right hand corner shows a vertically aligned magnetic texture and a strong magnetic contrast is found in the left SEMPA image. In the bottom left hand corner of the image the magnetic texture is aligned horizontally and only in the right SEMPA image a strong magnetic contrast is measured.

the m_y channel. The signal in the m_x channel shows a strong in-plane magnetization with a sinusoidal behavior for all measured angles, due to the spin spiral texture.

SIV. IN-PLANE SPIN SPIRAL ROTATING CW AND CCW

In this section we consider a different magnetic spin texture to the one presented in the main paper. Here, an in-plane rotating spin texture on the surface of FGT is discussed rotating in a clockwise as well as a counterclockwise fashion. We first focus on measurements on flake B depicted in Fig. S6a. The in-plane magnetization in the m_x direction is shown in the top SEMPA image and for m_y in the bottom SEMPA image. The area that is investigated in more detail is highlighted by the red outline and the averaged data in this area is plotted in Fig. S6b. A constant sinusoidal magnetic texture is obtained for the black data, corresponding to the m_x SEMPA image. The red data (m_y SEMPA image), however, shows an triangular shaped oscillatory behavior, which is shifted by a phase of $-\pi/2$ for negative x values and $+\pi/2$ for positive x values with respect to the m_x signal. We find that the sign of these phase shifts remains the same when α is rotated from $\alpha = -4°$ (Fig. S6b) to $\alpha = +9°$ (Fig. S6c). As discussed in the main paper, this indicates that the red data

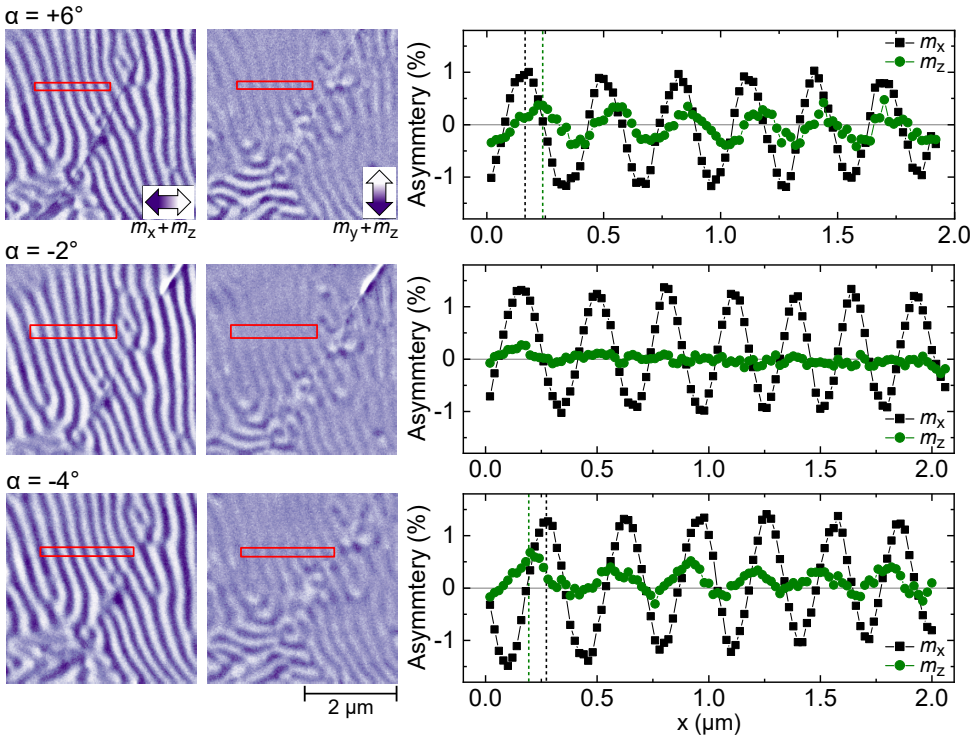

FIG. S5. SEMPA images on the flake A for $\alpha = +6°$ (top), $-2°$ (middle) and $-4°$ (bottom). The m_x SEMPA images (shown on the left) remain relatively unchanged for all tilt angles. The contrast in the m_y images (middle column) vanishes for $\alpha = -2°$. This is more clearly illustrated in the line traces shown in the right column of the channel asymmetry versus distance, averaged in the red boxes of the images. The change in phase shift indicated in the line traces for $\alpha = +6°$ and $\alpha = -4°$, and the vanishing signal in the m_y channel for $\alpha \approx 0$ is expected for a dominant out-of-plane signal in the m_y channel, as discussed in the main text.

points in Fig. S6b correspond mainly to the in-plane magnetization signal (m_y), rather than the out-of-plane component. We therefore observe an in-plane rotating spin texture with no apparent preferred sense of rotation at the surface of FGT. Moreover, the triangular shape of the m_y signal indicates, that the full magnetic texture is probably of a three-dimensional nature since the combination of the in-plane magnetic components do not result in a uniform magnetization.

The rotation direction of the spin texture can vary quickly in space and time, as can be seen in Fig. S7 in flake B. In Fig. S7a we show two SEMPA scans measured a few minutes apart, where the horizontal and vertical in-plane magnetization are depicted in the

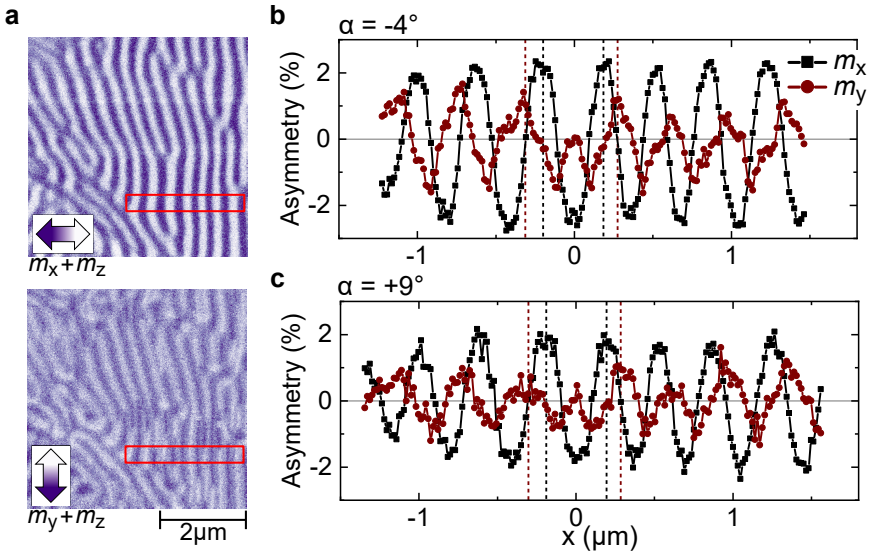

FIG. S6. **a** SEMPA images of flake B at $\alpha = -4°$ with the horizontal and vertical in-plane magnetization depicted in the top and bottom image, respectively. The red area is averaged along the vertical axis in **b**. A phase shift of $-\pi/2$ and $+\pi/2$ is observed between the m_x and m_y SEMPA data for negative and positive x. In **c** $\alpha = +9°$ and the phase shift remains the same as in **b**.

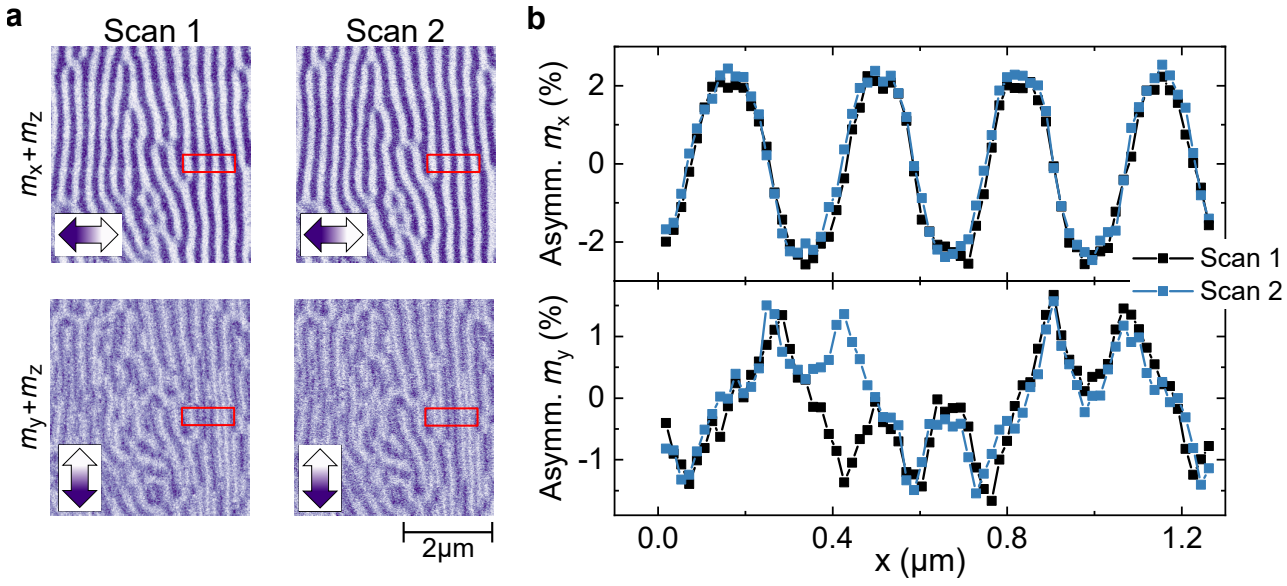

FIG. S7. **a** SEMPA images of two different SEMPA scans with the in-plane magnetization in the vertical direction and horizontal direction in the upper and lower row, respectively. **b** Averaged data for the m_x and m_y scan in the upper and lower panel, respectively. The signal in m_x is identical in both scans, but for the m_y scan the the magnetization changed sign around $x = 0.4$ μm.

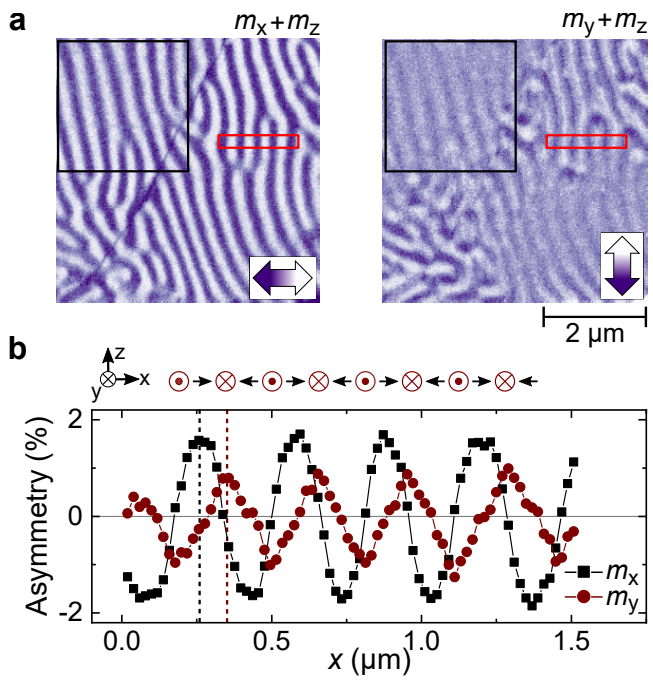

FIG. S8. **a** SEMPA image of flake A with the horizontal and vertical in-plane magnetization depicted in the left and right image, respectively. The area outlined in black is discussed in the main paper (Fig. 1). A different magnetization pattern becomes apparent in the upper right hand corner (mainly visible in m_y). The data outlined in red is plotted in **b** for the m_x (black data) and m_y (red data) magnetization. A schematic of the rotating magnetization in the xy-plane is illustrated on top of the panel.

upper and lower images, respectively. The data in the red area is averaged and plotted in Fig. S7b. The m_x signal shows a constant sinusoidal behavior, whereas the m_y shows a clear triangular shaped oscillatory behavior. At irregular intervals the phase shift between the m_x and m_y signal changes from $+\pi/2$ to $-\pi/2$. Moreover, in between two scans the phase shift changes locally, as can be seen around $x = 0.4$ μm. The simultaneous presence of both the clockwise and counterclockwise rotating in-plane spin texture and that the magnetic texture can change from one into the other over time indicate, that they are energetically similar at the surface of FGT.

Lastly we have a look at SEMPA measurements of flake A, depicted in Fig. S8a. In the main paper in Fig. 1 the area indicated by the black outline is discussed. Here, we focus on the area of the image in the upper right hand corner. In this region the same in-plane rotating magnetic texture is found as discussed in this section and the data outlined in red is

plotted in detail in Fig. S8b. From this measurement we find that the in-plane rotating spin textures can be present simultaneously with the counterclockwise Néel spin spirals (main paper Fig. 1) at the surface of bulk FGT.

SV. QUALITATIVE MICROMAGNETIC SIMULATIONS

The micromagnetic simulations in Fig. 2 of the main paper and this section are obtained with MuMax^3 [S3]. For all simulations the following settings were used. The cell sizes were (0.4, 8, 0.8) nm for (x, y, z) with periodic boundary conditions in the x- and y-direction for 32 repeats. The cell size in z corresponds to the height of a single FGT layer and in total 128 layers were simulated. A saturation magnetization of $M_{\mathrm{S}} = 0.38$ MAm^{-1} and an exchange stiffness of $A = 1$ pJm^{-1} were used [S4]. Additionally an interlayer exchange interaction was added with the strength of 10% of the exchange stiffness. We implemented this interaction via the RKKY interaction method discussed elsewhere [S4]. The anisotropy was varied from $K = 0.01 - 1.5$ MJm^{-3} and for every layer an interfacial DMI was added with a strength between $D = 0 - 0.8$ mJm^{-2}.

A magnetic domain texture was initialized in the following way: in total four alternating 'up' and 'down' domains were formed with $(m_{\mathrm{x}}, m_{\mathrm{y}}, m_{\mathrm{z}}) = (0.408, 0.408, \pm 0.816)$ and in between these domains 5 nm domain walls are initialized with $(m_{\mathrm{x}}, m_{\mathrm{y}}, m_{\mathrm{z}}) = (0.667, 0.667, 0.333)$. The simulations are minimized (using default settings) from the initialized state to obtain the equilibrium magnetization. For different simulation sets the signs of the initialized in-plane components of domains and/or domain walls are changed to check the consistency of the simulations. In Fig. 2c of the main paper the simulations shows a Bloch wall pointing in the $+y$-direction (blue color). However, a Bloch wall in the $-y$-direction (yellow color) would have the same energy. Both Bloch wall configurations are found in different simulations sets. This is not the case for Fig. 2d, however, where a finite D is present. For the indicated parameters all simulation sets show the same result, namely a counterclockwise rotating spin spiral.

Lastly we discuss the simulation results depicted in Fig. S9 that are in qualitative agreement with the in-plane magnetization texture discussed in Supplementary Section SIV. Here, the DMI is lower compared to the previous simulations, namely $D = 0.2$ mJm^{-2} and $K = 40$ kJm^{-3} and the upper panel of the figure shows the simulated magnetization

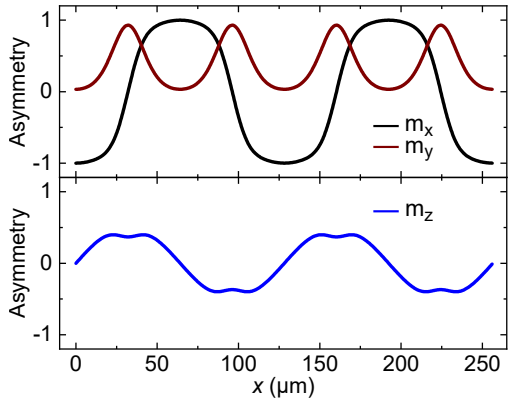

FIG. S9. Micromagnetic simulation of the surface magnetization of FGT for $D = 0.2$ mJm^{-2} and $K = 40$ kJm^{-3}. In the top panel the in-plane magnetic components are shown and the out-of-plane component in the lower panel.

profile of the top layer of FGT in the m_{x} and m_{y} direction in black and red, respectively. A sinusoidal pattern is found for m_{x} and the m_{y} signal peaks at every zero transition of m_{x}. The same behavior but for negative m_{y} values is found for a different simulation set. This magnetization profile (with either positive or negative m_{y} values) closely resembles the SEMPA images depicted in Fig. S7b. As was indicated, the overall structure is expected to be three dimensional and the simulated m_{z} component is plotted in the lower panel of Fig. S9.

Overall we find from Fig. 2c and d of the main paper and Fig. S9 that we are able to qualitatively simulate the different magnetic textures observed at the surface of FGT. However, the low anisotropy values and origin of a DMI remain elusive. A better understanding of several of the magnetic parameters and their thickness and temperature dependence would allow us to match the measured periodicity of the spin spiral to simulations and moreover to predict the magnetic texture of FGT.

[S1] R. Frömter, S. Hankemeier, H. P. Oepen, and J. Kirschner, Optimizing a low-energy electron diffraction spin-polarization analyzer for imaging of magnetic surface structures, Rev. Sci. Instrum. **82**, 033704 (2011).

[S2] J. Lucassen, *Exploring chiral magnetism with spin waves and domain walls*, Ph.D. thesis,

Department of Applied Physics (2020).

[S3] A. Vansteenkiste, J. Leliaert, M. Dvornik, M. Helsen, F. Garcia-Sanchez, and B. Van Waeyenberge, The design and verification of Mumax3, AIP Adv. **4**, 107133 (2014).

[S4] J. D. Clercq, J. Leliaert, and B. V. Waeyenberge, Modelling compensated antiferromagnetic interfaces with MuMax3, J. Phys. D: Appl. Phys. **50**, 425002 (2017).